Journal of the European Ceramic Society 46 (2026) 118051

Contents lists available at ScienceDirect

Journal of the European Ceramic Society

journal homepage: www.elsevier.com/locate/jeurceramsoc

Coupled evaluation of R-curve behaviour and subcritical crack growth: Experimental method and data interpretation

Marc Neumann [a,*], Hans Jelitto [b], Gerold A. Schneider [b], Christos G. Aneziris [a]

[a] Institute of Ceramics, Refractories and Composite Materials, Technical University Bergakademie Freiberg, Germany
[b] Institute of Advanced Ceramics, Hamburg University of Technology, Germany

ARTICLE INFO

Keywords:
Four-point bending
R-curve
Subcritical crack growth
Alumina
Silicon nitride

ABSTRACT

The fracture resistance is a design-relevant and material-specific feature. In ceramic materials, the fracture resistance can increase as a function of the crack length. Such behaviour is beneficial, e.g. in terms of the thermal shock resistance. It is termed R-curve behaviour and reflects the capacity of the material for intrinsic and/or extrinsic toughening during stable crack advance. Another design-relevant material-specific property is the sensitivity towards subcritical crack growth. The latter is a time-dependent phenomenon and commonly estimated by two crack growth parameters. The presented paper aims for a detailed review of sequential four-point bending experiments on V-notched beams, which are used to evaluate both phenomena from a single measurement. Three groups of materials (Al_2O_3, Si_3N_4, and Lithosil glass) were tested and analysed by this method in order to provide an experimental data background.

1. Introduction

For manifold purposes, the fracture behaviour of brittle materials is a design-relevant feature [1]. The linear elastic fracture mechanics with the stress intensity factor concept (also termed K-concept) is a powerful tool to describe the crack extension until fracture in brittle materials containing pre-existing defects. Such defects are often represented/symbolised by sharp cracks. The so-called stress intensity factor is introduced as a state variable and reflects the load amplification of an externally applied load leading to an applied stress σ in front of the crack tip inside the body. For tensile stresses, i.e. stress mode I, the stress intensity factor K in an edge-cracked body is written as [2]:

$$K_I = \sigma \Gamma \sqrt{a} \tag{1}$$

with Γ being a shape factor referring to the crack geometry and a being half of the crack length for a crack being inside the material or the full crack length if the crack starts on the surface of the sample. In a two-dimensional projection, a circular field evolves around the crack tip, which is solely determined by the stress intensity factor K_I. In a pre-cracked body under external loading, the stress intensity factor is increasing up to a critical level where crack extension is starting and [2,3]:

$$K_I = K_{Ic} \quad \text{with} \quad K_{Ic} = \sigma_c \Gamma \sqrt{a} \tag{2}$$

holds true. Such crack extension may accelerate until fracture, i.e. full separation into a minimum of two parts and thus catastrophic failure. This is referred to as unstable crack extension and in this case, the crack extends irrespective of the applied external load even if this load would be removed. The critical stress intensity factor K_{Ic} thus defines the condition for crack extension and is a material-specific quantity. Commonly, this critical stress intensity factor is termed fracture toughness [2]. In a wider sense it represents a measure for the crack resistance.

Apart from that, a crack may extend in stable manner meaning that the crack extension is governed by the applied load and could be arrested when the external load is removed or lowered. For different ceramic materials like alumina, zirconia, or silicon nitride, an increase in the crack resistance was observed during stable crack extension. This phenomenon is termed R-curve or R-curve behaviour and can be traced back to intrinsic or extrinsic toughening mechanisms [4,5]. The constant K_{Ic} then turns into $K_{IR} = f(\Delta a)$, being a function of the stable crack extension Δa. Remaining in the K-concept, the fracture criterion from Eq. (2) changes into Eq. (3): Unstable crack extension occurs at a constant external stress when the respective stress intensity factor K_I equals K_{IR} (Eq. (3a)) and when the respective stress intensity curve becomes a tangent (Eq. (3b)) [2].

$$K_I = K_{IR} \tag{3a}$$

and

$$\left.\frac{\partial K_I}{\partial a}\right|_{\sigma=\text{const.}} = \frac{dK_{IR}}{da} \tag{3b}$$

* Corresponding author.
E-mail address: marc.neumann@ikfvw.tu-freiberg.de (M. Neumann).

https://doi.org/10.1016/j.jeurceramsoc.2025.118051
Received 26 November 2024; Received in revised form 28 November 2025; Accepted 28 November 2025
Available online 29 November 2025

Another form of crack extension is the so-called subcritical cracking or subcritical crack growth. Depending on the time available and at stress intensity factors below K_{Ic} or K_{IR}, pre-existing cracks may grow too, leading to postponed failure as soon as the crack length reaches critical values. This phenomenon is the so-called subcritical cracking or subcritical crack growth. Material-specifically, subcritical crack growth is exclusively dependent on the effective stress intensity factor. In approximation, the crack growth rate $v = da/dt = f(K_I)$ is a function of the current stress intensity and can be written as [2]:

$$v = \frac{da}{dt} = AK_I^n = A^* \left(\frac{K_I}{K_{Ic}} \right)^n \quad (4)$$

where A, A^*, and n are material specific parameters. All three of the parameters A, A^*, and n further depend on the humidity, on the ambient temperature, and on whether external load is applied in static or cyclic manner. Often, the dimensionless exponent n (also termed subcritical crack growth exponent) is used to describe the sensitivity towards subcritical crack growth. The higher the exponent n, the lower is the sensitivity (i.e. the tendency) to subcritical crack growth [2]. As proven for alumina, the subcritical crack growth behaviour can be influenced by the R-curve, and vice versa [6–8]. Following Eq. (4), the parameter A^* relates to the fracture toughness K_{Ic}. Consequently, when the material shows an R-curve K_{IR} instead of a constant fracture toughness K_{Ic}, the reference value below the fraction line evolves with the overall crack extension. This is hard to evaluate experimentally with a sufficient accuracy. For this reason, the focus is put on the parameter A, which applies irrespective the circumstance whether the material shows a constant fracture toughness or an R-curve.

Throughout literature numerous methods to evaluate the R-curve or the subcritical crack growth behaviour are known. Mostly, these methods are time-consuming and may require a high number of samples (such as in static or dynamic life-time-measurements), or they may require complex sample geometries or test set ups (such as the wedge-splitting-, double-cantilever-beam-, or double-torsion-test) [2,9–12]. Another issue may be a lack in terms of the data resolution during the crack initiation. This paper summarises the merits and limits of a time-efficient sequential four-point bending method with a high data acquisition rate, designed for the coupled evaluation of both the R-curve and the subcritical crack growth in brittle materials. Insights into the experimental setup, data acquisition, and data processing are included, while all data processing is possible and was done in the free software package 'R' (version 4.4.1) [13]. This method has already been used in the recent past for various ceramic materials, e.g. including ZrB_2–SiC [14] or flame-sprayed Al_2O_3–ZrO_2–TiO_2 compounds [15].

2. Experimental procedure

2.1. Materials and sample preparation

Two ceramic materials were investigated: alumina Al_2O_3 and silicon nitride Si_3N_4. Subclasses were formed, depending on the sintering regime (Al_2O_3) or the specifications of the manufacturer (Si_3N_4). For comparison, a single sample of Lithosil glass was tested as well. Glass is known to show no R-curve behaviour and thus serves as a test, whether stable crack growth can be initiated in a non-toughening material. An overview on the test series is provided in Table 1.

Beams of $3 \times 4 \times 45$ mm^3 ($b \times w \times l$) were required for the bending experiments. In the case of the Al_2O_3 series, blanks were prepared from fine powder (Taimei DAR, TKK Taimei Chemicals Co., Ltd, Japan) employing a sequence of cold uniaxial pressing at 30 MPa and cold isostatic pressing at 500 MPa. The fabricated blanks were then sintered and ultimately processed into beams of the above-mentioned dimensions. Due to the powder particle sizes (0.21 µm on average) and the compaction during the pressing and sintering, the relative density of the alumina materials is assumed to be close to 1. The Si_3N_4 samples were supplied by FCT Ingenieurkeramik GmbH (Germany) and were tested in the as-received state. According to the manufacturer, the Si_3N_4 materials show a residual porosity of less than 1 vol%. Lastly, the Lithosil glass sample was provided by Schott AG (Germany) and also tested as-received. Table 2 lists the basic physical properties of the materials investigated. The mean particle sizes of the Al_2O_3 series after sintering were evaluated by means of optical microscopy utilising a polarising filter and small aperture in order to highlight diffraction effects at the grain boundaries (Leitz Aristomet optical microscope). However, this was successful only for the alumina series A, B, and C. Holding the premise that the elastic behaviour of dense ceramic materials is determined by the chemical composition and since the alumina samples were all fabricated from the identical alumina raw powder, the Young's modulus of the Al_2O_3 series was assumed with $E = 393$ GPa. This was evaluated from static bending tests on an unnotched B-Al_2O_3 beam. The Poisson ratio was approximated to be $\nu = 0.2$ for all materials. Since the influence of the Poisson ratio is rather low (cf. Eqs. (5) and (10)), this is considered a minor in-accuracy. However, a more precise evaluation of the Poisson ratio in the advance of the measurement would definitely be advantageous and is recommended.

A V-notch was polished into each sample, which served as a starting point for crack growth. A relative notch depth of 0.50 to 0.60 (50 % to 60 %) was needed (notch depth divided by sample thickness). First, a U-notch was cut by means of a diamond cutting wheel with a total width of 150 µm to a relative depth of about 0.40 (40 %). Afterwards, the V-notch was polished into a V-shape and its final depth by the aid of razor blades, covered with diamond pastes. This was done in a graded manner, starting with a diamond paste with a mean particle size of 6 µm and finishing with a paste with a mean particle size of 1 µm. The final notch depth was measured optically on the sample surface. Detailed theoretical considerations on the required relative notch depth, i.e. the minimum notch depth required for stable crack growth, are included in Appendix A to this paper.

2.2. Mechanical testing

All bending tests were performed in a specially designed four-point bending machine at the Institute of Advanced Ceramics, Hamburg University of Technology (AC-TUHH) at room temperature (50 % to 60 % relative humidity). Each beam sample was always mounted in a way that the V-notch opening faced the side which was subjected to tensile stress. The support roller spans were $s_1 = 20$ mm and $s_2 = 40$ mm. The machine compliance of the entire set up amounted to 0.065 µm N^{-1} (measured at 50 N). Prior to the testing, the installed sample was clamped with a pre-load of 4 N. Subsequently, two position encoders were mounted at the tensile-stressed sample face, one at the centre (right next to the notch) and one near one of the lower support rollers. The reason for the two position encoders is that the pure bending (deflection) of the sample can be measured without the deflection due to the compression of rollers and parts of the machine. Next, the sample was loaded and unloaded five times in a range of 1 N to 8 N, to minimise potential settling effects at the moveable support rollers. After this, the computer-controlled sequential bending was initiated, which was realised via LabVIEW. From that point, the sample was loaded till the current slope of load vs. deflection dropped below a limit criterion. If the slope, being the stiffness of the sample, decreases, it means that the crack has started to grow. Then, the sample was partially unloaded, i.e. released, which was followed by the next sequence and so forth. The loading parts of these sequences are further denoted as load sequences. The current load–deflection-slope was evaluated as the tangent slope to the last 15 load–deflection-data points. The limiting slope criterion had to be adjusted in the course of the bending experiment, since this slope naturally evolved with the number of loading-unloading sequences, thus related to the crack length [16]. The load was applied with a controlled deflection rate of 0.02 µm s^{-1}. Due to this low deflection rate, an experiment may take 1 h to 4 h depending on the material. The unloading was realised at 10 µm s^{-1}.

Table 1
Investigated materials (AC: Institute of Advanced Ceramics, Hamburg University of Technology; all manufacturers from Germany)

Material	Subclass	Manufacturer	Preparation/Remark	Samples
Al_2O_3	A	AC	Cold pressing (uniaxial and isostatic) Sintering: 1350 °C for 2 h	2
Al_2O_3	B	AC	Cold pressing (uniaxial and isostatic) Sintering: 1600 °C for 1 h	2
Al_2O_3	C	AC	Cold pressing (uniaxial and isostatic) Sintering: 1600 °C for 96 h	2
Al_2O_3	D	AC	Cold Pressing (uniaxial and isostatic) Sintering: 1500 °C for 1 h	1
Si_3N_4	GP	FCT Ingenieurkeramik GmbH	Gas Pressure Sintering tested as-received	3
Si_3N_4	PU	FCT Ingenieurkeramik GmbH	Hot Isostatic Pressing tested as-received	3
Lithosil		Schott AG	tested as-received	1

Table 2
Physical properties of the tested materials.

Test Series	Mean Particle Size in µm	Young's modulus in GPa
A-Al_2O_3	1–2	393
B-Al_2O_3	5–8	393
C-Al_2O_3	10–12	393
D-Al_2O_3	–	393
Si_3N_4-GP	1–15[a]	290[a]
Si_3N_4-PU	1–10[a]	320[a]
Lithosil	–	72[a]

[a] According to manufacturer.

In the course of the whole measurement, the load F_{exp}, time t, and experimental deflection δ were recorded. The latter was calculated from the difference of both position encoders using beam theory [17]. A quartz dynamic load cell 9212 of Kistler Instrument GmbH (sensitivity of $-11.3\,pC\,N^{-1}$) was used as load sensor for the high resolution load measurements. The load sensor tended to drift over time, which had to be corrected for each sample individually. For this purpose, the samples were unloaded completely about every 20-30 min. The used position encoders (WI/2mm-T, Hottinger Baldwin Messtechnik GmbH, Germany) had a measuring range from −58 µm to 58 µm. The data acquisition was governed by an adjustable load–deflection-databox, which was set to 0.03 µm × 0.3 N. Whenever the absolute difference of the current load or deflection and the previously stored data point exceeded the respective box size, the current F_{exp}-δ-t-data is saved as the new data point. This databox prevents data being recorded continuously when force and displacement are constant for a while.

In order to determine the crack length, the calculatory compliance method is applied according to Section 3. Another option would be an optical crack length evaluation at the specimen surface via microscope. However, there are some restrictions in relying on the optically measured crack length: the visibility of the optical crack length is highly dependent on the degree of polishing possible for the investigated material. Besides, the optical crack length at the sample surface may be affected by a curvature of the crack front, which is likely to occur after the notching with razor blades and diamond pastes. That would lead to a misestimation, while the compliance method models an averaged crack front across the entire sample cross section. For those reasons the compliance was preferred over the optical measurement.

3. Refinement and interpretation of load–deflection-time data

3.1. Data terminology

Prior to the actual evaluation of the R-curve or the vK_I-data the machine raw data had to be corrected for the drift in the recorded load F_{exp} on the basis of the complete unloadings. Since this is beyond the scope of this paper, the correction of the load drift is omitted here, but is included in Appendix B. From this point on, all subsequent steps of data processing are referring to the load drift corrected data either in the form of the corrected load F over δ or F over t. As mentioned, a complete data set consists of several individual load sequences and since of no further need other than the load drift correction, the limbs of complete unloading can be removed from the data, cf. Fig. 1(a). Remaining in the $F\delta$-plot, a typical shape of an isolated load sequence is presented in Fig. 1(b). As shown, a load sequence is divided into two parts, a linear and a nonlinear portion separated by a transition point (trs) and comes with an initial (init) and release point (rls).

3.2. Calculation of the crack length

The relative crack length a_r can be evaluated from the sample compliance $C(a_r)$ as follows: for an increasing relative crack length the compliance increases as well, for a constant compliance, the crack extension would be arrested. Hence the compliance is a function of the crack length. An equation for this relationship, which is applicable to four-point bending, was established by Munz and Fett [2,14,17,18]:

$$C(a_r) = \frac{9(s_2 - s_1)^2}{2E'bw^2} \int_0^{a_r} \frac{a'(\Gamma_M(a'))^2}{(1-a')^3}\, da' + C_0^* \tag{5a}$$

$$C_0^* = \left(\frac{s_2 - s_1}{w}\right)^2 \frac{1}{E'b}\left(\frac{s_2 + 2s_1}{4w} + \frac{(1+\nu)w}{2(s_2+s_1)}\right) \tag{5b}$$

$$\Gamma_M(a_r) = \Gamma(1-a_r)^{1.5} = 1.1215\sqrt{\pi}\left[\frac{5}{8} - \frac{5}{12}a_r + \frac{1}{8}a_r^2 + 5a_r^2(1-a_r)^6 + \frac{3}{8}\exp\left(-6.1342\frac{a_r}{(1-a_r)}\right)\right] \tag{5c}$$

Since plain strain conditions apply, E' reads as $E' = E/(1-\nu^2)$ [14, 17]. In order to calculate an explicit relative crack length of interest $a_{r,x}$, $C(a_r)$ needs to be substituted by the respective experimental compliance C_{meas} in Eq. (5). The most basic definition of the compliance C is $C = \Delta\delta/\Delta F$, thus the inverse of a slope ζ in the $F\delta$-display. However, owed to the real world testing situation, the experimental compliance C_{meas} cannot be taken directly as this inverse. For the common 20 mm-40 mm-four-point-bending test setup and the positions of the two deflection sensors, C_{meas} is defined by Eq. (6), with $\zeta = \Delta F/\Delta\delta$[17]. The specific slope ζ depends upon which property is of interest (subcritical crack growth parameters or R-curve behaviour).

$$C_{meas} = 2/3\zeta^{-1} + 0.4479C_0^* \tag{6}$$

The calculation of the relative crack length of interest $a_{r,x}$ is done by iterating the upper integration limit in Eq. (5) in small steps, until the resulting $C(a_r)$ exceeds the experimental compliance C_{meas}. Then, the last iteration of a_r before the integral $C(a_r) > C_{meas}$ is considered as the respective relative crack length of interest $a_{r,x}$ at C_{meas}. In the present study, the step width between the iterations is fixed to 0.0001. The calculatory effort may be reduced by setting the first iteration point to the relative notch depth (approximately 0.5). The integral itself must be solved numerically (in this study by a Gauss–Kronrod quadrature).

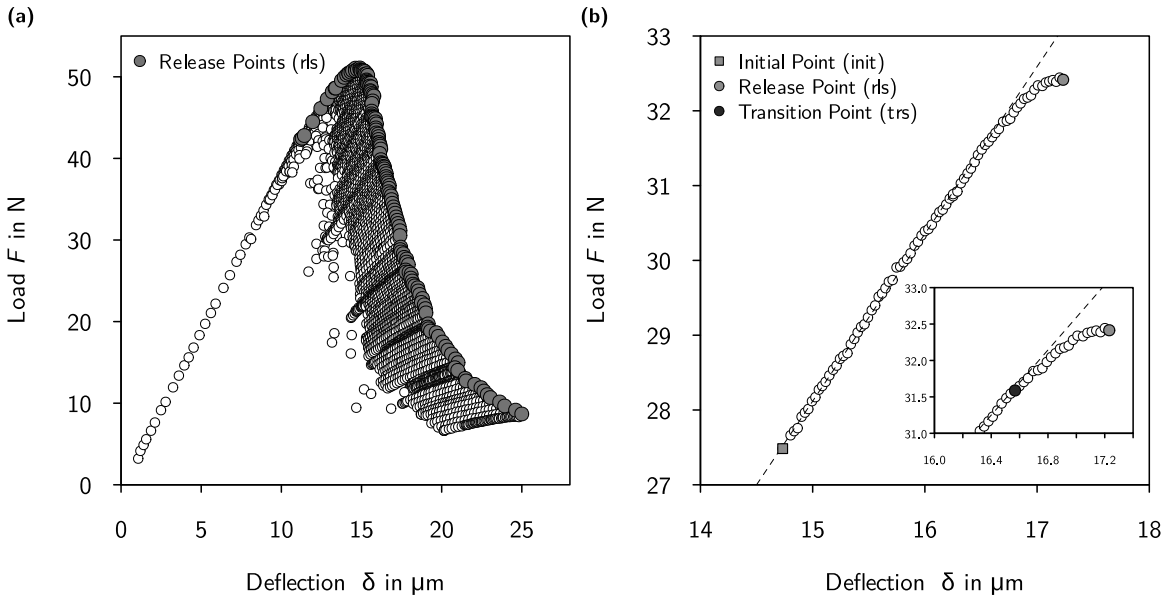

Fig. 1. Corrected load–deflection-data after removing the limbs of complete unloading (a) and exemplarily isolated load sequence (b). All based on sequential four-point bending on an Si_3N_4-PU-sample.

Eventually, the relative crack length a_r and the absolute crack length a are related via $a_r = a/w$.

This method of calculation provides a mean crack length over the through-thickness crack, originating from the sharpened notch ground. Hence, it accounts for a non-uniform crack front to some extend.[1] An optical crack length observation, mostly done on one side of the sample only, tends to underestimate the crack length in the sample volume, especially when starting from a curved or skewed notch ground [19]. Another advantage is the fact that Eq. (5) applies to relative crack lengths from 0 to 1, thus a vast range of crack extension is granted access to. Related to the resolution of the $F\delta$-data, this method may further come with a very fine resolution regarding the crack length, which is helpful especially during the initiation of the stably growing crack. Downsides of the compliance-method are its sensitivity, for instance towards locally varying material elasticity due to microstructural variation (Young's modulus), and that a very stiff, nearly non-compliant testing device is required. The latter was indeed given in case of the bending device at the TUHH [16,20].

3.3. R-curve-behaviour

The R-curve can be derived by correlating the crack length at the release points with the corresponding stress intensity factor. Thus, the release compliance C_{rls} of each individual sequence is introduced into Eq. (5):

$$C(a_r) \mathrel{\hat{=}} C_{rls} = 2/3\zeta_{rls}^{-1} + 0.4479C_0^* \tag{7}$$

Hence, the release slope ζ_{rls} is required, which can be determined as the linear slope between the release point of a sequence i and the initial point of the following sequence $i+1$ (cf. Fig. 2):

$$\zeta_{rls} = \frac{F|^i_{rls} - F|^{i+1}_{init}}{\delta|^i_{rls} - \delta|^{i+1}_{init}} \tag{8}$$

In principle, the respective release and initial points can be selected graphically using the plot of the load F against the time t. Similarly, plotting the load F over the data point index would be possible, too. A graphic display of the choice of the release and initial points by the aid of the time t, and the resulting release slope is shown in Fig. 2(a) for one exemplary release. Despite already removed, it should be noted that the limbs of complete unloading must be skipped, since they represent a manual interference. For an overall visualisation, Fig. 1(a) additionally shows the emphasised curve of release points, superposed on all raw data in grey.

In Fig. 3(a), the resulting release slopes ζ_{rls} are presented over the sequence index number. Likewise is the resulting release compliance C_{rls}. Ultimately, the release slopes ζ_{rls} decreased over the course of the experiment, which means an increase in the release compliance C_{rls} and thus an increase in the crack length a. In Fig. 3(b), crack length a and crack extension Δa after the load releases at the end of the sequences are displayed over the evolving release compliance C_{rls}. The crack extension was derived by subtracting the optically determined notch depth from the absolute crack length a. For the known crack length and the load in the release points, the corresponding stress intensity factor was calculated according to Eq. (9) and is further referred to as K_{IR} as said before. Ultimately, the typical R-curve-diagram can be derived by plotting K_{IR} against Δa, see Fig. 3(c).

$$K_I = \frac{F}{b\sqrt{w}} \frac{s_2 - s_1}{w} \frac{3\sqrt{a_r}}{2(1-a_r)^{1.5}} \Gamma_M(a_r) \tag{9}$$

Since the notch depth is determined by optical microscopy, the following should be noted: when calculating Δa using this optically evaluated notch depth, an offset of the R-curve towards higher initial Δa could be observed. Potential reasons trace back to an inconsistent (curved) notch front. That may have several reasons, especially when the notch preparation is performed with razor blades. The following effects and their combinations can be considered the major reasons:

[1] Considering the stress conditions along the whole crack front more closely, plane stress conditions apply near the surface of the sample, while plane strain conditions apply at the crack front inside the beam sample. Consequently, the crack front is slightly curved and the crack length inside the sample is larger than on its surface. Thus, if testing with optical crack length observation and if the crack becomes visible on the surface of a material with a steep R-curve, the plateau of the R-curve is almost reached and the steep initial increase cannot be measured. The automated control by recording the change of the compliance readily allows for the measurement of the steeply rising R-curve of materials. An example for a material with a very steep R-curve is in fact Si_3N_4.

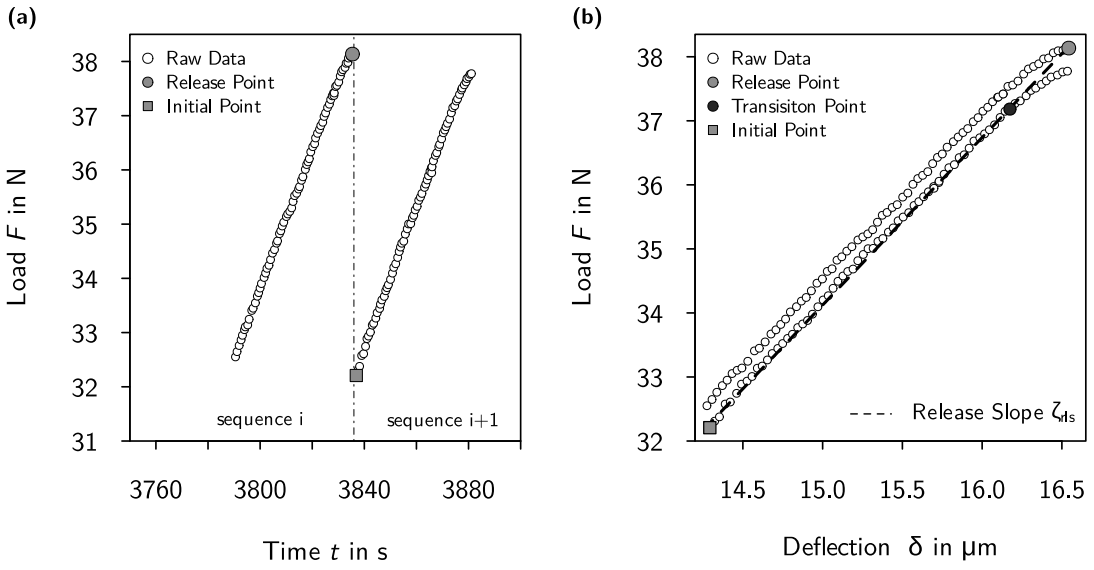

Fig. 2. Extraction of release and initial points of the load sequences on the basis of the load-time-data (a) and resulting release slopes ζ_{rls} (b). All based on sequential four-point bending of an Si_3N_4-PU-sample.

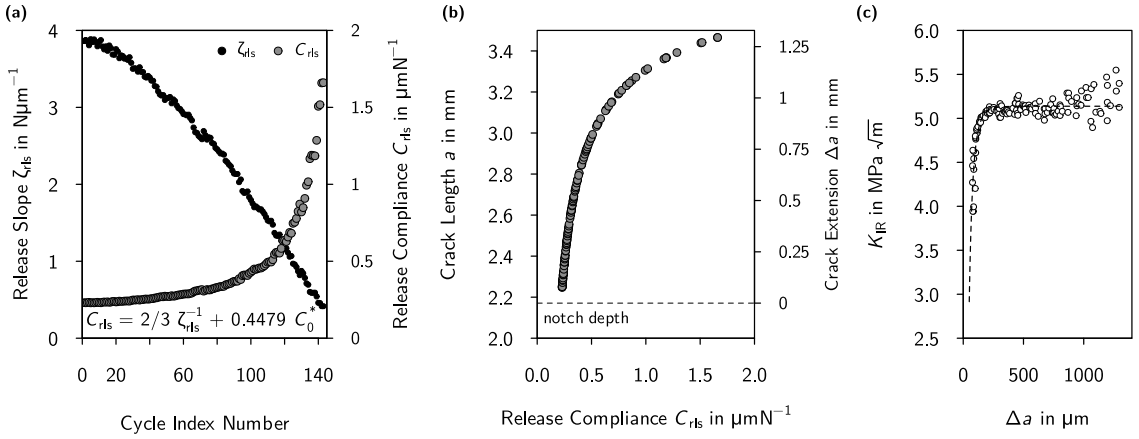

Fig. 3. Resulting unloading slopes ζ_{rls} and compliances C_{rls} (a), crack length calculation on the basis of C_{rls} (b), and resulting R-curve (c), all based on sequential four-point bending of an Si_3N_4-PU-sample.

- Slight inaccuracies of the sample shape result in a tilted positioning below the razor blade and thus in a slightly tilted notch front in the first place.
- Inconsistent wear of the employed razor blades may cause a curved notch ground/front.
- During the notching procedure, a certain region ahead of the notch front could be damaged. That would appear even more pronounced for already weakened structures, containing micro-cracks or other micro-voids.
- A specific point of the presented study is the Young's modulus. As stated, a general Young's modulus is assumed per test series/material (cf. Table 1). The very specific Young's modulus of an individual sample may differ from that value, which would affect the R-curve [18]. However, the impact of this fact is expected to stay behind the first three phenomena, since the difference in the Young's modulus is rather low (±5 GPa at maximum).

Differences between the optically measured and the maximum internal crack length calculated from the sample compliance were investigated by Özcoban et al. [19] For the present study, an offset of (275 ± 8) µm was derived as a criterion for correction. Any offset significantly higher than 275 µm demands for an alternative correction, i.e. adjusting the underlying Young's modulus. Insofar the initial offset of the R-curve was smaller than 275 µm, an apparent notch depth was set so that the R-curve starts at 0 µm of crack extension.

3.4. Subcritical crack growth

The phenomenon of subcritical crack growth can be evaluated by extracting and analysing individual load sequences in terms of $F = f(\delta, t)$ [14]. The aim was to derive the crack extension rate v over the stress intensity factor K_I, thus to evaluate the parameters n and A (cf. Eq. (4)). Referring to Fig. 1(b), the non-linear sequence portion, flanked by the transition and the release point, results from subcritical crack extension. Accordingly, the crack length for each data point of the non-linear part was calculated on the basis of the sample compliance, only that the change of compliance $\Delta C(a_r)$ was used.

Since the difference $\Delta C(a_r)$ was considered, the absolute term of C_0^* lapsed. The integration limits represent the initial crack length of the sequence (lower integration limit) and the crack length in a data point of the non-linear portion (upper integration limit). For the linear sequence portion, where no change of compliance exists, the

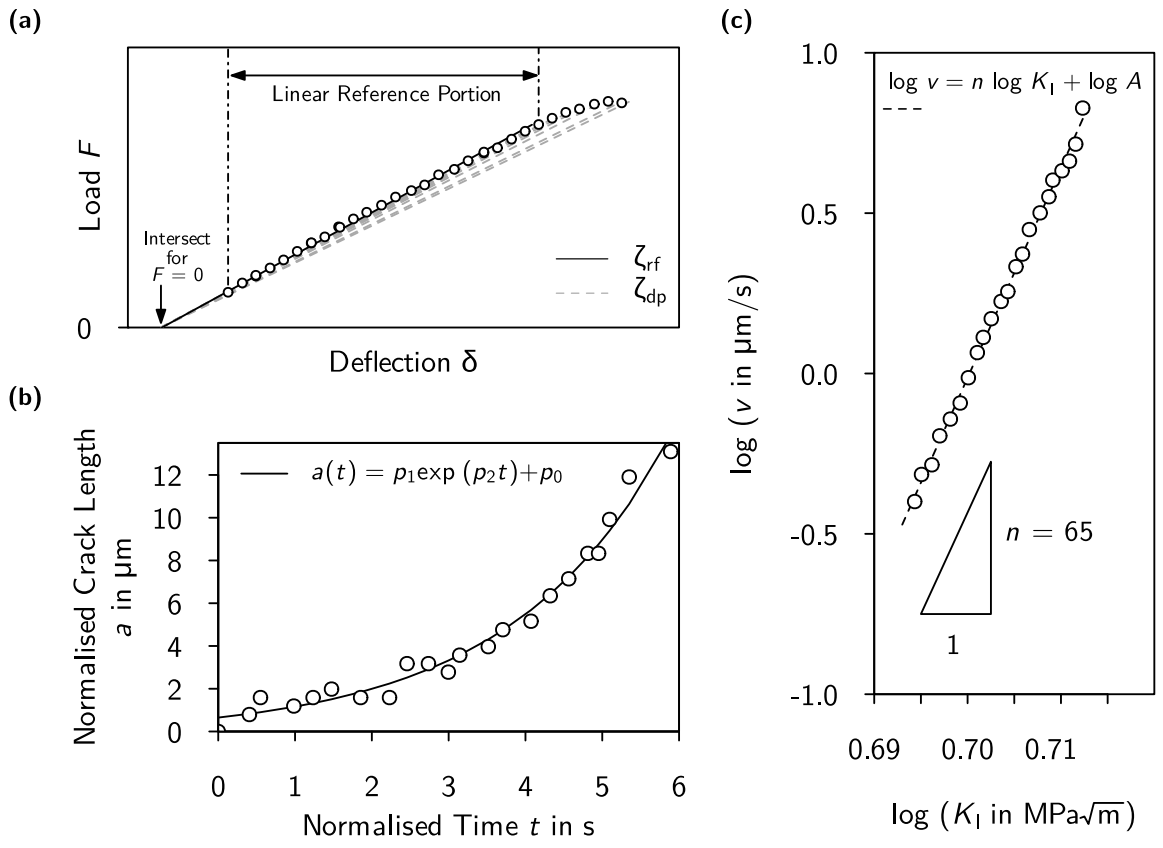

Fig. 4. Schematic illustration of the fundamental load–deflection characteristics for $\upsilon - K_I$ analysis in one load sequence (a), exemplary results of crack length over time, derived from the non-linear portion of one load sequence (b) and the corresponding crack growth rate over the stress intensity factor (c); all based on sequential four-point bending of an Si_3N_4-PU-sample.

crack length is constant and complies with the initial crack length of the selected sequence. The slope ζ_{rf} of this portion (reference slope) is determined by linear fitting of all data points between the initial and the transition point (cf. Fig. 4(a), solid line). The change in the compliance for each data point of the non-linear portion was evaluated from the change in the data point slope ζ_{dp} (cf. Fig. 4(a), dashed lines). These were derived as the slopes between the data point itself and the x-axis intersect of the linear fit of the linear reference portion. The change of the compliance $\Delta C \propto (\zeta_{rf} - \zeta_{dp})^{-1}$, fed into Eq. (10), was determined taking into account Eq. (6).

$$\Delta C(a_r) = \frac{9(s_2 - s_1)^2}{2E'bw^2} \int_{a_{r,a}}^{a_{r,b}} \frac{a'(\Gamma_M(a'))^2}{(1-a')^3}\, da' \tag{10}$$

Subsequent to that, the crack length a can be normalised for the initial crack length of the sequence and plotted over the time t. The data was normalised for the absolute time value of the transition point for convenience, see Fig. 4(b). Insofar present, crack extension (under subcritical loads) can be seen. For further evaluation, the normalised crack length a over time t can be fitted, e.g. by an exponential equation:

$$a(t) = p_1 \exp(p_2 t) + p_0 \tag{11}$$

Its first derivative according to the time t provides the crack growth rate υ. Furthermore, the stress intensity factor K_I can be calculated per point, again by Eq. (9). The resulting υK_I-data now allowed for linear fitting (when plotted in a logarithmic display) and the parameters n (also visualised as the slope) and the parameter A can be derived, cf. Fig. 4(c). Since one single measurement comprises several of such load sequences, statistics can be accounted for by considering several sequences per sample and several samples in total. In conjunction to the R-curve data processing and as a measure of adequacy of the employed methods, the initial crack length of a sequence i and the crack length in the release point of the preceding sequence $i-1$ should be the same. This is fulfilled insofar the release slope of the sequence $i-1$ and the reference slope of the sequence i are the same. A visual representation of that is presented in Fig. 2(b).

3.5. Methodological limits

Conclusively, the stable crack growth experiments hold the advantage to derive several characteristics from one measurement. Thus, the applied testing method has to be seen as superposition of individual phenomena, i.e. the subcritical crack growth and the R-curve behaviour. Both mutually influence each other [2,6]. Besides, the used sequential loading is considered to have a certain impact on the R-curve behaviour itself. For alumina materials, several studies found that sequential load application degrades potential toughening mechanisms, such as crack tip shielding or crack bridging [7,8]. Gilbert et al. [7] derived a decreased shielding capacity of crack bridging zones in the crack wake due to friction wear of the bridges as direct consequence of cyclic loads. Further experimental insight was provided by El Attaoui et al. [8], where after switching from a static to a cyclic load application, the R-curve dropped and did not reach crack resistances measured during static loading. That behaviour was again interpreted as degradation of the crack tip shielding. Hence, sequential load application during an experiment is considered to cause an underestimation of the R-curve. According to Danzer et al. [1] also fatigue may influence the R-curve in a similar way. Since such an underestimation would represent a more cautious approach, it is not necessarily considered adverse.

In terms of the subcritical crack growth, the following statements should be given: The span of crack growth rates υ was rather narrow when compared to υK_I-data, presented elsewhere [1,8]. In the present study it could be observed though that for pure alumina materials

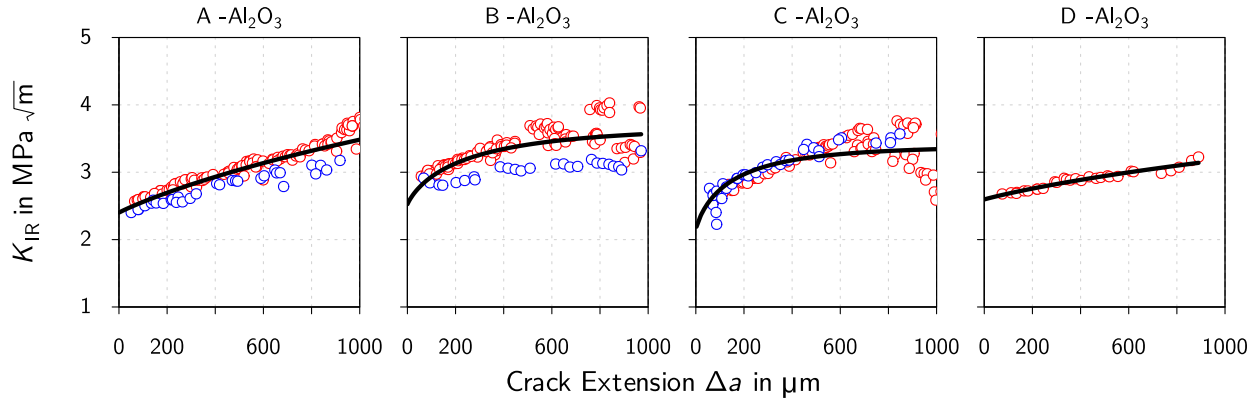

Fig. 5. Resulting R-curves for the tested Al_2O_3 materials, cumulatively fitted by an exponential model from the literature (solid black line; coloured plot symbols indicate different samples per material).

the crack growth exponents n resulting from such narrow spans of the crack growth rate v matched the scale of literature values from other test procedures (cf. Section 3.6). Therefore, the employed method is considered suitable to evaluate the scale of the subcritical crack growth parameters. Moreover, since the presented method was employed equally for each sample of this study, the comparability among the materials is given. Still, the determined values should be treated as estimates and be given together with a scatter estimation.[2]

3.6. Material evaluation and comparison

The resulting R-curves of the individual Al_2O_3 series A, B, C, and D are presented in Fig. 5. The data was cumulatively fitted by an exponential model with three free parameters K_{I0}^{mod}, q, and p (cf. Eq. (12)) [21].

$$K_{IR} = K_{I0}^{mod} + q\left[1 - (1 + p\sqrt{\Delta a})\ \exp(-p\sqrt{\Delta a})\right] \tag{12}$$

The scale of the Al_2O_3 R-curves matched data published on the subject before [4,22]. The R-curve was not fully developed within the first 1000 µm of crack extension for A- and D-Al_2O_3, while the R-curves of B- and C-Al_2O_3 reached their plateau after approximately 600 µm to 800 µm of crack extension. In general, the Al_2O_3 R-curves showed a rather mild to modest increase, stretched over several hundred micrometres, like observed before as well [4,22]. Potentially, they may span several millimetres of crack extension [4,22–24]. Hence, the presented experimental setup and data processing routine could be employed successfully to evaluate the R-curve of materials with a mildly to modestly ascending crack resistance. Potential mechanisms causing such an R-curve behaviour in alumina are the deflection of the crack path alongside the grain boundaries and crack surface friction effects (bridging) [22,25].

In contrast to that, silicon nitride Si_3N_4 is expected to show a steep R-curve, which is characterised by a steep increase within the first micrometres of stable crack extension. The plateau value of K_{IR} is then reached after just a few hundred micrometres [26–32]. Consequentially, a high resolution in terms of the stable crack extension is required for such materials, especially at the crack initiation. In fact such a resolution can be provided by the presented experimental technique and as demonstrated in Fig. 6, a steep R-curve could be determined for both tested Si_3N_4 materials (and for all samples). Through fitting by the same exponential model, already employed for Al_2O_3, it was revealed that for either the Si_3N_4-GP or the Si_3N_4-PU the plateau was reached after approximately 300 µm of stable crack extension. However, the plateau value differed and amounted to about 5.8 MPa $\sqrt{m}$ and 5.0 MPa $\sqrt{m}$ for Si_3N_4-GP and Si_3N_4-PU, respectively. The slight shift towards initial crack extensions greater than zero might stem from a curved notch front and/or from using the data sheet Young's modulus [18,19]. However, the influence of the latter is assumed to be minor in comparison to the impact of the curved notch front. In sum, the presented experimental setup and data processing routine also allow for the evaluation of the R-curve of materials with a steeply ascending crack resistance. Thus, the employed fit model appeared to be suited to adapt for both cases as well (mild or steep ascend) [21]. The acting mechanisms causing the R-curve behaviour in Si_3N_4 were profoundly discussed by Fünfschilling et al. [21] As outlined, it is a multiple-stage process involving elastic bridges without debonding, elastic bridges that are partially debonded, and frictional bridges at last [21].

Finally, Fig. 7(a) shows the resulting 'R-curve' of the tested Lithosil glass sample. A drop in K_{IR} in the first 200 µm of crack extension and then a rather constant (i.e. flat) 'R-curve' instead of an ascending trend were revealed. These elevated K_{IR} values during the crack initiation may stem from the creation of an atomically sharp tip from the rounded notch ground with its finite notch root radius, the so-called notch effect [33–35]. Özcoban et al. [33] had studied this notch effect on notched Si_3N_4 beams: For the creation of an atomic sharp crack tip, a nominal load was observed, which was higher than the actually necessary maximum load (i.e. when the notch effect would be absent). Accordingly, the shape of the $F\delta$-curve would alter. Assuming a constant fracture resistance without any R-curve effects, a schematic of that alteration is added in Fig. 7(b) [33]. In fact, such an altered shape of the $F\delta$-data was observed for the glass material (cf. black circles in Fig. 7(b)).[3] Eventually, that could be translated into the acting stress intensities. For visualisation, hyperbolas of constant stress intensity were added to the $F\delta$-data (coloured lines). The elevation of K_{IR} at crack initiation from Fig. 7(a) is now well reflected in the

[2] By testing at various deflection rates, for instance measuring at two or three different levels during one experiment (e.g. at 0.02 µ ms^{-1} and 0.12 µ ms^{-1}; several load sequences for each level) or measuring several samples of the same material but at different deflection rate levels, different sections of the potential vK_I-curve could be observed. These can be combined to provide a more comprehensive picture of the whole vK_I-data.

[3] The influence of the notch effect upon the $F\delta$-data was not observed for either of the ceramic materials (cf. the $F\delta$-data presented in Fig. B.14(c) as a typical example). In fact, the ceramic samples were prepared similarly to the glass sample meaning they had a finite notch radius as well. Since the ceramic materials had a polycrystalline microstructure, individual gussets or cavities at the grain boundaries in the immediate vicinity of the notch tip may act as an 'apparent' notch radius in the nanometre range, to some extend minimising the notch effect.

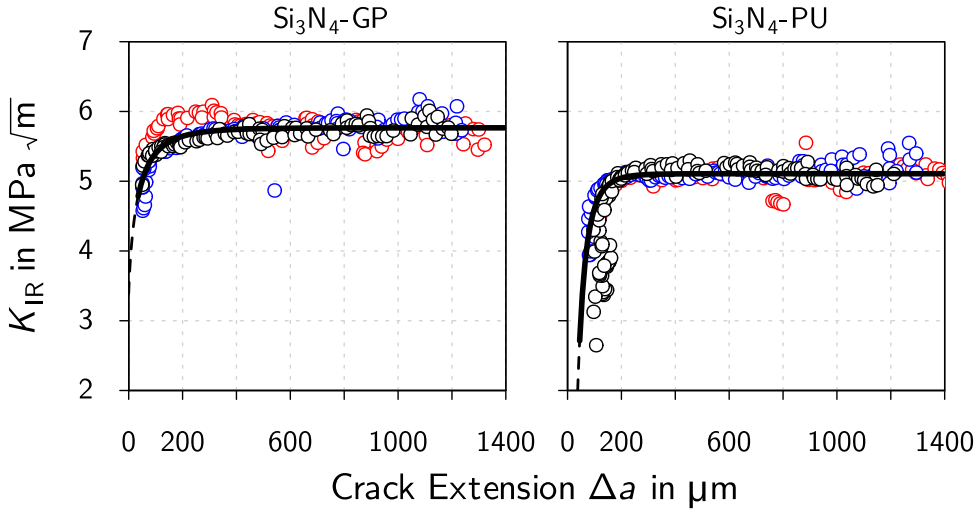

Fig. 6. Resulting R-curves for the tested Si_3N_4 materials, cumulatively fitted by an exponential model from the literature (solid black line; coloured plot symbols indicate different samples per material; dashed line segments indicate extrapolated model towards $\Delta a = 0\,\mu m$).

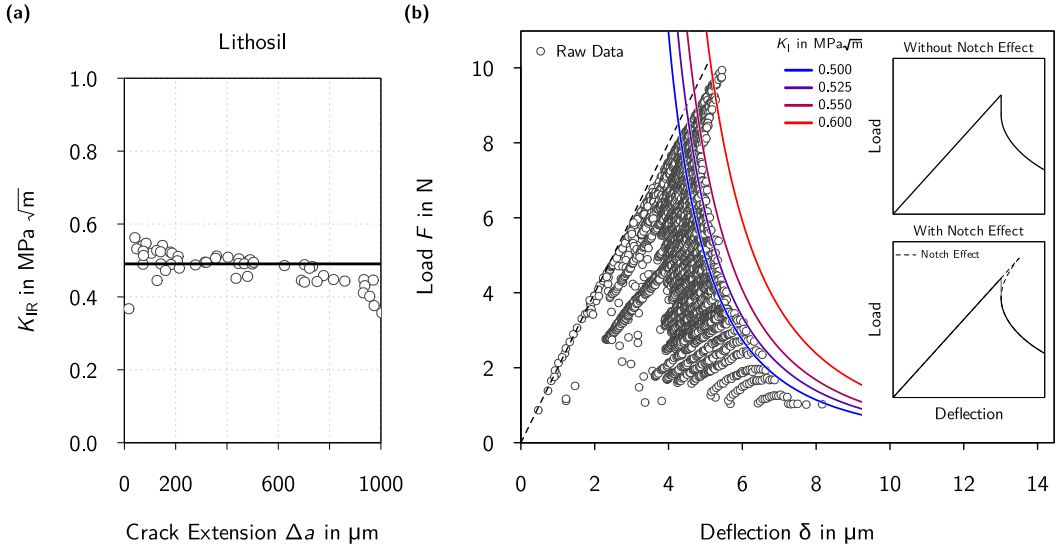

Fig. 7. Resulting R-curve for the tested Lithosil glass (a), 'fitted' by the median value (solid black line), and hyperbolas of constant stress intensity K_I superimposed to the load–deflection-raw data and including a schematic of the influence of the notch effect on the load–deflection-data during crack initiation [33](b).

$F\delta$-data: The region close to the maximum loads, i.e. the right flank i.e. the curve of releases first complies/intersects hyperbolas of higher stress intensities of $K_I \geq 0.550\,\text{MPa}\sqrt{\text{m}}$, before aligning with hyperbolas of $K_I \simeq 0.515\,\text{MPa}\sqrt{\text{m}}$. That is in good agreement to the level of K_{IR} of the 'R-curve' from Fig. 7(a).[4] Then the approximately constant level of the crack resistance aligns with the observations from previous stable crack growth experiments on glass at comparable relative crack lengths [36]. Consequently, despite the lack of any sort of toughening and the elevation of the stress intensity during the crack initiation, it was possible to initiate, drive, and control a stably growing crack, since a change in the compliance was indeed observed. Due to the constant level of K_{IR}, fitting by an intricate model is not necessary, the data is well reflected by the median (solid black line) and matches the general scale of the fracture toughnesses of glasses from previous studies [37–39]. The crack initiation, i.e. the first 200 µm of crack

[4] The hyperbolas were derived from Eq. (5), Eq. (6), and Eq. (9) assuming purely linear-elastic behaviour, i.e. assuming that full releases would end at the origin of the $F\delta$-diagram (0 µm,0 N). As a consequence, the imaginary line of the release for purely elastic behaviour would always result from the linear connection between the release point and the origin point at 0 µm and 0 N. Due to inelastic processes, potentially occurring in the real world sample, full releases would not end at the origin but at deflections δ larger than 0 µm. If this is the case, the release slope would be higher than the theoretical slope for purely elastic behaviour. Accordingly, the resulting stress intensities would be lower in the 'not-fully' elastic behaving material/sample. In the presented routine, that is accounted for by approximating the release slope at each release point from the release point itself and the onset of the consecutive load sequence. That causes the slight mismatch between the levels of K_{IR} in Fig. 7(a) and the theoretical stress intensity curves, presented in the $F\delta$-diagram in Fig. 7(b). The latter still visualise the notch effect properly and were thus added.

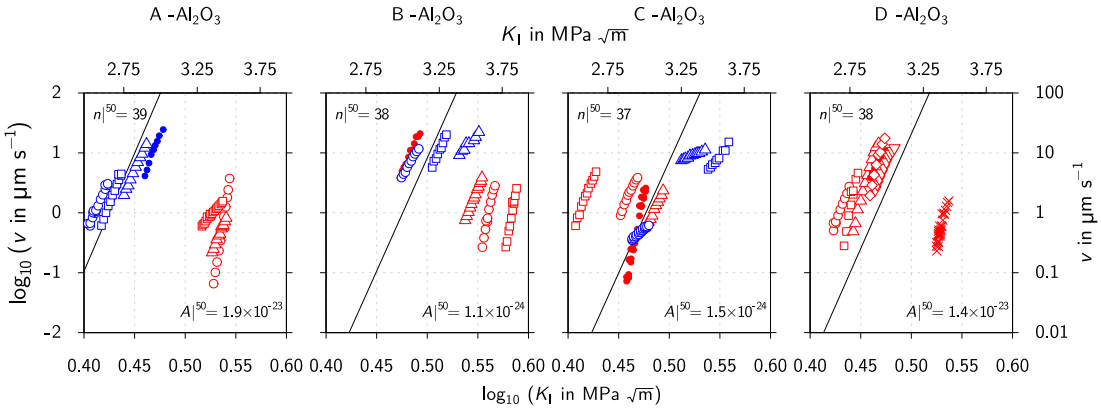

Fig. 8. Exemplary vK_I-data of the respective alumina series, extracted from individual load sequences of the stable crack growth experiments (colour code matches the presented R-curve raw data of the investigated alumina materials). The solid lines show averaged linear fitting based on all individual load sequences per material (seven sequences are presented as examples per material; $n|^{50}$ represents the median crack growth exponent; $A|^{50}$ in $(\mathrm{m\,s^{-1}})(\mathrm{MPa}\sqrt{m})^{-n}$).

Table 3
Quartiles $|^{25}$, $|^{50}$, and $|^{75}$ of the subcritical crack growth parameters of the investigated materials (parenthesis next to the name of the test series list the number of investigated sequences of the respective material; n dimensionless, A in $(\mathrm{m\,s^{-1}})(\mathrm{MPa}\sqrt{m})^{-n}$; $|^{50}$ denotes the median value).

	A-Al_2O_3[28]	B-Al_2O_3[29]	C-Al_2O_3[23]	D-Al_2O_3[14]	Si_3N_4-GP[45]	Si_3N_4-PU[45]	Lithosil[15]
$n\|^{25}$	19	21	16	6	66	70	18
$n\|^{50}$	39	38	37	38	80	83	27
$n\|^{75}$	47	58	50	64	91	98	44
$A\|^{25}$	2.9×10^{-31}	3.0×10^{-42}	6.7×10^{-31}	2.7×10^{-34}	6.8×10^{-76}	9.0×10^{-77}	1.4×10^{1}
$A\|^{50}$	1.9×10^{-23}	1.1×10^{-24}	1.5×10^{-24}	1.4×10^{-23}	1.9×10^{-66}	3.3×10^{-65}	2.5×10^{3}
$A\|^{75}$	4.1×10^{-17}	2.5×10^{-16}	2.5×10^{-14}	2.3×10^{-8}	2.1×10^{-57}	8.9×10^{-56}	5.6×10^{11}

extension, was excluded from the median calculation for the 'R-curve'-fitting to eliminate the chance for overestimation due to the notch effect.

Turning to the subcritical crack growth behaviour, examples for the resulting vK_I-curves of the Al_2O_3 series are presented in Fig. 8. A fit line is added, calculated from the median $n|^{50}$ and $A|^{50}$ per test series. In accordance to the literature, the data is presented in a log–log display and thus linearised. The vK_I-analysis was done for a minimum of 10 sequences per sample. Exemplarily, the results of 7 randomly chosen sequences per material are presented per subfigure in Fig. 8.

As a statistical measure, the quartiles of the derived parameters n and A are listed in Table 3. According to the derived exponents $n|^{50}$, the sensitivity towards subcritical crack growth was approximately the same for all of the Al_2O_3 series. The scattering of the parameter n was most pronounced for D-Al_2O_3, i.e. it appeared higher than it was for any of the other Al_2O_3 series. Against the background of the experimental method described, a high variation in n may be attributed to a high microstructural variation along the cross-section of the samples [14]. One reason for this could be a non-optimal compaction during the sample preparation. Another reason could be the superposition of the subcritical cracking and the R-curve behaviour, i.e. a more complex material behaviour. Nevertheless, the data presented is a valid approach for benchmarking the alumina materials against previous studies. In comparison to literature data (see Table 4), the resulting crack growth exponents n of the current study match the data reported for Al_2O_3. Thus, the coupling of the analysis of the R-curve and the subcritical crack growth was successful for Al_2O_3, i.e. the literature data could be reproduced reliably. Besides the efforts in the experimental time and the sample material could be reduced drastically in the present method.

The resulting vK_I-curves of the Si_3N_4 series are shown in Fig. 9, again linearised, i.e. presented in a log–log display. Both Si_3N_4 materials resemble each other in terms of the subcritical crack growth

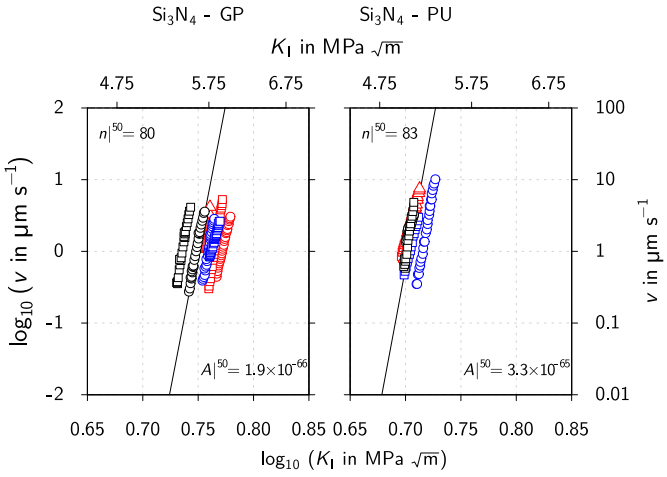

Fig. 9. Exemplary vK_I-data of the respective silicon nitride series, extracted from individual load sequences of the stable crack growth experiments (colour code matches the presented R-curve raw data of the investigated silicon nitride materials). The solid lines show averaged linear fitting based on all individual load sequences per material (seven sequences are presented as examples per material; $n|^{50}$ represents the median crack growth exponent; $A|^{50}$ in $(\mathrm{m\,s^{-1}})(\mathrm{MPa}\sqrt{m})^{-n}$).

with median exponents of $n|^{50} = 80$ and $n|^{50} = 83$ for Si_3N_4-GP and Si_3N_4-PU, respectively. Therefore, the sensitivity towards subcritical cracking is rather low when compared to Al_2O_3 ($n|^{50}_{Si_3N_4} > n|^{50}_{Al_2O_3}$). Consequently, despite the differences in the subcritical cracking behaviour, both cases (intermediate and low sensitivity) could be analysed and mapped successfully using the same experimental setup. Literature data

Table 4
Literature based values of crack growth exponent n of alumina, silicon nitride, and glass materials at room temperature in air (n dimensionless; whenever the experiments were not performed in air, it is specified in parenthesis).

Material	Test Mode	Reference	Parameter
Al_2O_3	not specified	[40]	$n = 31$
Al_2O_3	not specified	[41]	$n = 28.9$
Al_2O_3	static	[42]	$n = 33 \pm 5$
Al_2O_3	cyclic	[42]	$n = 27 \pm 5$
Al_2O_3	cyclic	[43]	$n = 28.2$–34.2
Al_2O_3	static	[43]	$n = 38.6$
Al_2O_3	static (in salt water solution)	[44]	$n = 20.0$–73.5
Al_2O_3	cyclic	[7]	$n = 16$–47
Al_2O_3	not specified	[1]	$n = 33$
Si_3N_4	not specified	[45]	$n = 12$–18
Si_3N_4	dynamic	[46]	$n \simeq 30$
Si_3N_4	dynamic	[47]	$n \simeq 30$
Si_3N_4	not-specified	[48]	$n \simeq 30$
Si_3N_4	dynamic	[49]	$n = 16.2$–20.3
Borosilicate glass	static (in water)	[50]	$n = 14$
Borosilicate glass	static (in water)	[51]	$n = 15$
Borosilicate glass	static (in water)	[52]	$n = 15$
Soda-Lime-Silicate glass	static (in water)	[40]	$n = 14.0$–14.2
Soda-Lime-Silicate glass	static (in vacuum)	[53]	$n \simeq 90$
Fused Silica glass	static (in water vapour)	[54]	$n \simeq 31$

from flame-sprayed alumina-rich materials revealed that materials with high sensitivity towards subcritical cracking ($n < 15$) could be analysed as well, thus the full spectrum is covered [15]. The literature data found for Si_3N_4 listed exponents n two to three times lower than those found for Si_3N_4-GP and Si_3N_4-PU, cf. Table 4. This may trace back to several reasons, foremost differences in the material manufacturing (shaping technology, sintering time, temperature, additives/constituents, sintering kinetics due to impurities etc.). Besides, as discussed earlier, the possibly observable ranges of the subcritical crack growth rate v are to some extend limited for the present experimental set up, especially at a constant rate of loading. By varying the rate of loading over the course of the experiment, this range could be extended. As the data was processed in the same way as for the Al_2O_3 series, which was found to be in sound agreement with the literature, the parameters derived from the Si_3N_4 series are considered to be reliable characteristic values for Si_3N_4-GP and Si_3N_4-PU.

Finally, the vK_I-data of the Lithosil sample is presented in Fig. 10. In terms of the crack growth exponent n the Lithosil glass resembles the results of the Al_2O_3 series, but clearly at considerably lower stress intensities (scaling according to the R-curves, cf. Figs. 5 and 7(a)). Literature reports on glasses often refer to subcritical crack growth experiments in water resulting in crack growth exponents of $n \simeq 14$–15 (cf. the values for borosilicate or soda-lime-glass in water in Table 4). That indicates a high sensitivity to subcritical cracking, such as that for intensely microcracked ceramics [15]. However, in vacuum, crack growth exponents of $n \simeq 90$ were observed [53]. From that Wiederhorn et al. [53] stated that for the presence of water, the crack growth exponent n would decrease by a factor of about 2 to 10. In fact, Suratwala et al. [54] found values in water vapour near $n \simeq 30$ (0.3 Pa water vapour pressure, N_2-atmosphere), which is in good agreement to the present data collected in moist air. Thus, as a proof of concept, also glass can be analysed in terms of both the crack resistance and the subcritical crack growth behaviour, revealing reliable data.

A closing word in terms of the subcritical crack growth data shall be given to the scaling parameter A. Recalling the logarithmic form of Eq. (4), i.e. $\log v = n \log K_I + \log A$, the parameter estimation of A is rather sensitive to a variation in the exponent n, regardless of how small this variation would be, due to the logarithm. Differences in n may change the order of magnitude of A. However, previous studies have shown that it is still feasible to employ the derived A, e.g. in lifetime prediction [15]. Thus, they are presented in Table 3 for the sake of integrity. For alumina, the data generally matches the scale of A from the literature [7]. However, hardly any or no data can be found for the other two materials, so this comparison is omitted at the present time.

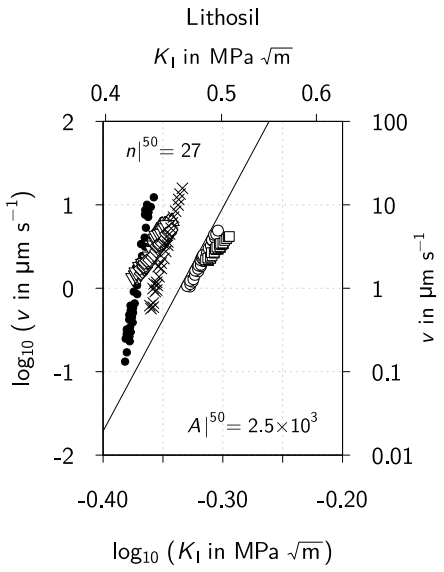

Fig. 10. Exemplary vK_I-data of the Lithosil glass, extracted from the individual load sequences of the stable crack growth experiment (colour code matches the presented R-curve raw data of the Lithosil glass). The solid lines show averaged linear fitting based on all individual load sequences of the material (seven sequences are presented as examples per material; $n|^{50}$ represents the median crack growth exponent; $A|^{50}$ in $(\mathrm{m\,s^{-1}})(\mathrm{MPa}\sqrt{m})^{-n}$).

4. Conclusion

The present paper demonstrates a sequential four-point-bending method for the fracture mechanical characterisation of brittle solid materials such as ceramics or glass and the respective data processing. By performing loading-unloading sequences (i.e. load sequences) on a V-notched bending beam, it was possible to initiate and control a stably growing crack from the notch ground. The recording of load, deflection, and time allowed for the evaluation of the R-curve behaviour and subcritical crack growth phenomena, if present in the tested material. The advantages of the sequential testing are:

- The preparation of a bending beam is relatively simple, i.e. easier than that of a compact tension sample.
- The R-curve and subcritical crack growth can be measured simultaneously and in a relatively short time span on a single notched bending beam.
- The experiment is computer controlled, which eases the control of the stable crack advance and allows for a high-resolution data acquisition.
- The computer-control drastically facilitates stable crack advance, because due to the compliance method the computer already visualises/detects crack extension, even if crack advance is not visible on the sample's surface.

The data processing routine and the methodological limits are described in detail using three fundamentally different materials as examples: alumina, silicon nitride, and glass. For all investigated materials, the bending experiments could be performed successfully and the resulting data was summarised and compared to the literature. It could be verified that the presented method is suitable to characterise both the

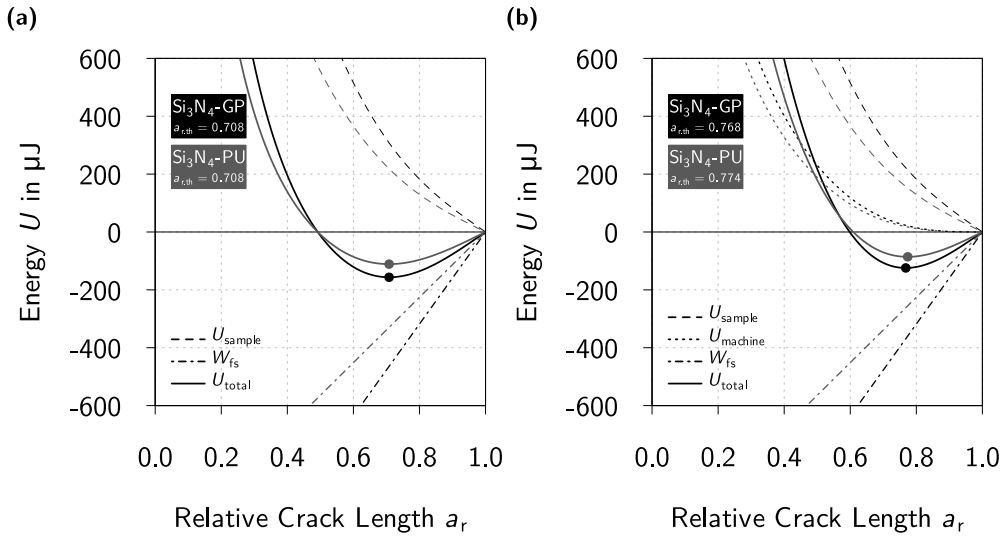

Fig. A.11. Energy balance during 20/40 mm four-point-bending for $C_m = 0\,\mu m/N$ (a) and $C_m = 0.065\,\mu m/N$ (b).

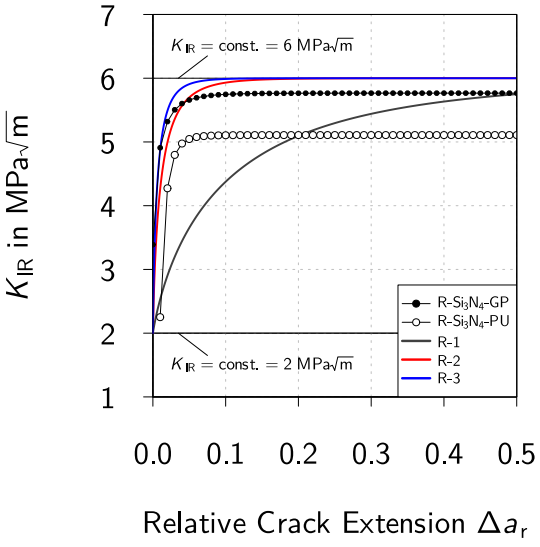

Fig. A.12. Assumed R-curves R-1, R-2, and R-3 (solid lines), based on literature data for the minimum and maximum K_{IR} and different steepnesses for Si_3N_4[55]. The black and the white dot-lines represent the R-curves of the investigated Si_3N_4-GP- and Si_3N_4-PU-material.

crack resistance (i.e. the R-curve behaviour) and the subcritical crack growth behaviour for all of the materials within the corresponding framework of the data known from the literature.

CRediT authorship contribution statement

Marc Neumann: Writing – review & editing, Writing – original draft, Visualization, Validation, Software, Methodology, Formal analysis, Conceptualization. **Hans Jelitto:** Writing – review & editing, Validation, Methodology, Investigation, Formal analysis, Data curation, Conceptualization. **Gerold A. Schneider:** Writing – review & editing, Supervision, Resources, Project administration, Funding acquisition, Conceptualization. **Christos G. Aneziris:** Writing – review & editing, Supervision, Resources, Project administration, Funding acquisition, Conceptualization.

Declaration of competing interest

The authors declare that they have no known competing financial interests or personal relationships that could have appeared to influence the work reported in this paper.

Acknowledgements

The authors thank J. Krivohlavek and A. Lenhardt for their comprehensive efforts in terms of sample preparation, notch preparation, data curation, and foremost the testing, as well as A. Borchert for sample fabrication and H. Özcoban for internal discussion. The authors would also like to express their sincere thanks to R. Janssen for his advice, support, and all the valuable discussions.

Appendix A. Crack stability

A necessary precondition for the evaluation of R-curve behaviour and /or subcritical crack growth is to allow for stable crack extension. Nakayama et al. [56] addressed this phenomenon in their paper on the reliability of work-of-fracture experiments performed on notched beam samples. The key to ensure stable crack growth is the notch depth and is derived from the energetic balance during the bending experiment. It thus relates to the energy concept outlined in the introduction of the present paper. According to Nakayama et al. [56], the energy balance during a uniaxial bending test reads as:

$$U_{total} = U_{sample} + U_{machine} + W_{fs} + U_{kinetic} \tag{A.1}$$

introducing U_{total} as the total energy of the bending system, U_{sample} and $U_{machine}$ as the elastically stored energy in the beam sample and the bending machine, W_{fs} as the work required for fracture, and $U_{kinetic}$ as a kinetic energy term. For the given rates of loading during the present testing procedure (cf. experimental section), $U_{kinetic} = 0$ can be assumed. The work required for fracture follows as (S total crack area created during fracture) [2,56]:

$$W_{fs} = -2\gamma S = -G_c S = -G_c\,(1 - a_r)\,wb = -\frac{K_{Ic}^2}{E'}\,(1 - a_r)\,wb \tag{A.2}$$

and $U_{sample} + U_{machine}$ can be defined as [2,56]:

$$U_{sample} + U_{machine} = \frac{1}{2}F^2C(a_r) + \frac{1}{2}F^2C_m \tag{A.3}$$

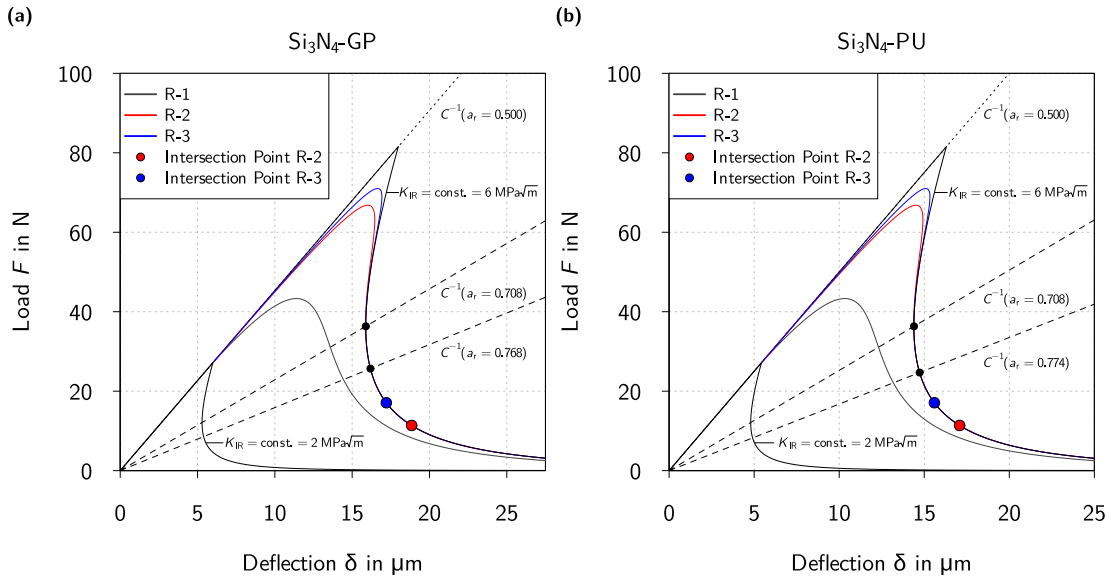

Fig. A.13. $F\delta$-curve on the basis of the Si_3N_4-GP (a) and Si_3N_4-PU (b) material data from Table A.5 for the assumed crack resistances and R-curves from Fig. A.12. Black dots indicate intersects between the compliance-lines (dashed lines; derived from the thresholds from Fig. A.11) and the $F\delta$-curve for K_{IR} = const. = 6 MPa $\sqrt{m}$. Colour-coded dots indicate intersects between the theoretical $F\delta$-curves for the assumed R-curves R-2 and R-3 and the $F\delta$-curve for K_{IR} = const. = 6 MPa $\sqrt{m}$ (according to the respective colour-coding). For the hypothetical samples, a relative notch depth of $a_{r,nd} = 0.50$ was assumed (dotted line).

Table A.5
Assumed material data, sample geometry, and support spans (E and K_{Ic} according to manufacturer).

Material	E in GPa	K_{Ic} in MPa $\sqrt{m}$	ν	b in mm	w in mm	s_1 in mm	s_2 in mm
Si_3N_4-GP	290.0	6.2	0.2	3.0	4.0	20.0	40.0
Si_3N_4-PU	320.0	5.6	0.2	3.0	4.0	20.0	40.0

where C_m represents the machine compliance. For the presented experimental setup, $C(a_r)$ is given by Eq. (5), while F can be derived from Eq. (9) as:

$$F = \frac{2K_{Ic}b\sqrt{w}w(1-a_r)^{1.5}}{3(s_2-s_1)\Gamma_M(a_r)\sqrt{a_r}} \tag{A.4}$$

Exemplarily, the crack stability situation shall be calculated for Si_3N_4-GP and Si_3N_4-PU assuming the material and sample data from Table A.5. In a first approximation, C_m can be neglected, i.e. $C_m = 0$. The resulting energy balance is plotted in Fig. A.11(a). The energy balance curve, additionally including the machine compliance, is presented in Fig. A.11(b). For the present set up, a machine compliance of $C_m = 0.065$ µm/N could be measured in compressive tests at 50 N.

According to Nakayama et al. [56], stable crack growth is possible when $dU/da_r \geq 0$. Then the criterion for stable crack growth can be derived as follows: To ensure stable crack growth, the required minimum threshold notch depth $a_{r,th}$ corresponds to the minimum in the total system energy curve U_{total}. In Fig. A.11, the minimum points are highlighted by dots. Neglecting the machine compliance, i.e. for $C_m = 0$, the minimum threshold notch depth $a_{r,th}$ is independent of the fracture toughness and the Young's modulus (cf. Fig. A.11(a)). When accounting for the machine compliance, i.e. for $C_m \neq 0$, the threshold notch depths $a_{r,th}$ are no longer independent of the fracture toughness and are shifted towards higher values.

In the present case, relative threshold notch depths of $a_{r,th} \geq 0.7$ were revealed. The experimental notch depths $a_{r,nd}$ for the Si_3N_4-GP- and Si_3N_4-PU-samples were in a range of $0.50 < a_{r,nd} < 0.55$, i.e. lower than the theoretical thresholds. However, stable crack growth was in fact observed for all of the samples. This stems from the fact that both Si_3N_4-materials showed an increasing R-curve. Theoretically, due to R-curve behaviour, i.e. due to toughening mechanisms, stable crack extension could be possible even for $a_{r,nd} < a_{r,th}$ [57].

Table A.6
Assumed R-curve model parameters for R-1, R-2, R-3 (based on Eq. (12))

R-curve	K_{I0}^{mod} in MPa $\sqrt{m}$	q in MPa $\sqrt{m}$	p in $\sqrt{m}^{-1}$
R-1	2	4	100
R-2	2	4	300
R-3	2	4	400

In sound agreement with the literature, the R-curve of Si_3N_4 can be approximated between a minimum K_{IR} = 2 MPa $\sqrt{m}$ and a maximum K_{IR} = 6 MPa $\sqrt{m}$ [55]. For the present calculations, three differently sloped R-curves were assumed, cf. R-1, R-2, and R-3 from Fig. A.12. Those were found by introducing the parameters from Table A.6 into Eq. (12). It should be noted that R-1 with its broad stretch is rather unusual for Si_3N_4, yet it shall serve only for comparison purposes.

The crack resistances from Fig. A.12 (K_{IR} = 2 MPa $\sqrt{m}$, K_{IR} = 6 MPa $\sqrt{m}$ as well as R-1, R-2, R-3) were translated into $F\delta$-curves, which are plotted in Fig. A.13. Hypothetical samples with a relative notch depth of $a_{r,nd} = 0.50$ were assumed (represented by the dotted line, remaining sample characteristics as in Table A.5). Besides, the threshold values from Fig. A.11 were added as a line with a constant slope of $C^{-1}(a_{r,th})$ (dashed lines).

For samples without any toughening, i.e. with a constant crack resistance, unstable failure would occur as soon as the maximum critical load for crack initiation is reached, represented by the black solid lines for K_{IR} = 2 MPa $\sqrt{m}$ and K_{IR} = 6 MPa $\sqrt{m}$ and their immediate drop after reaching the maximum load. For samples with an increasing R-curve, crack initiation would start at the critical peak load corresponding to the minimum K_{IR}, in this case to K_{IR} = 2 MPa $\sqrt{m}$. Due to the toughening effects, more energy is required to 'overcome' the toughening and hence the load is still increasing beyond that point.

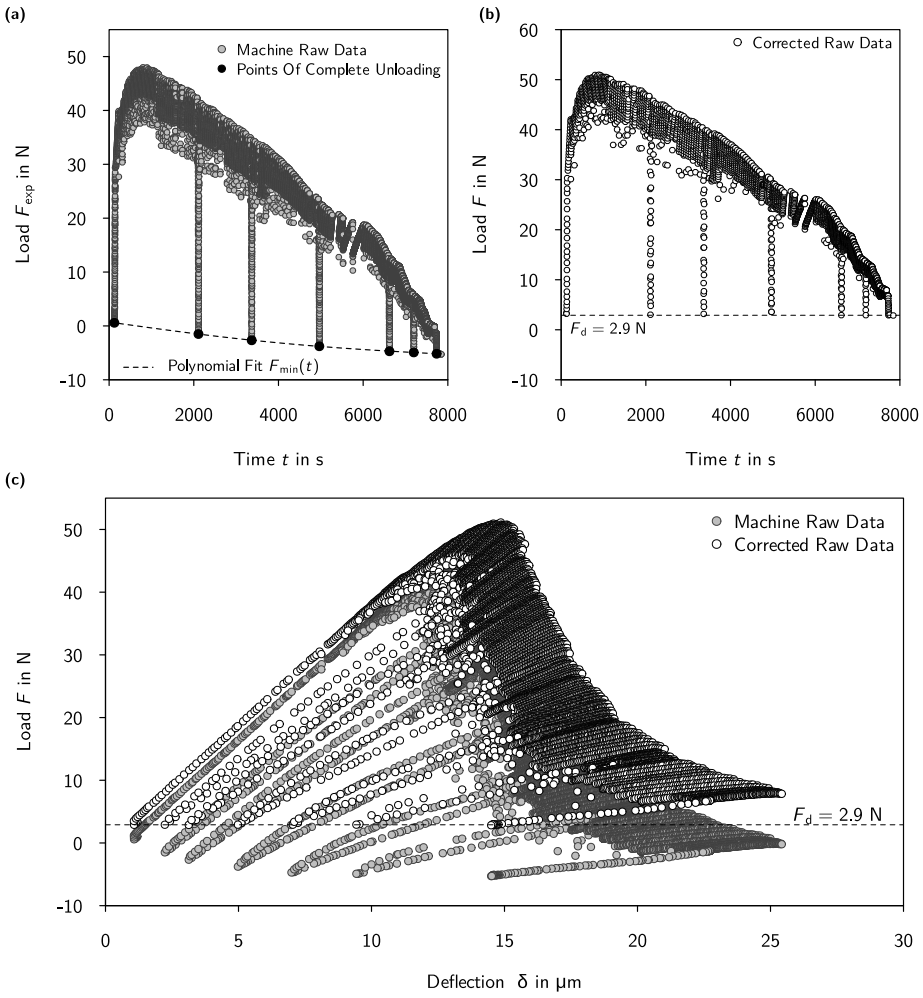

Fig. B.14. Machine raw data: load F_{exp} vs. time t and emphasised points of complete unloading (a). Data correction: load F vs. time t (b) and load F vs. deflection δ (c), all based on sequential four-point bending on an Si_3N_4-PU-sample.

As a consequence, the crack is extending stably until the $F\delta$-curve intersects the theoretical $F\delta$-curve for the maximum K_{IR} of the R-curve, in this case for $K_{IR} = 6\,\text{MPa}\sqrt{\text{m}}$. As long as this intersect is located behind the intersects of the threshold lines and $F\delta$-curve for $K_{IR} = 6\,\text{MPa}\sqrt{\text{m}}$, stability is ensured despite $a_{r.nd} < a_{r.th}$ [57].

In Fig. A.13 it is illustrated best by the $F\delta$-curve for R-1. Such an R-curve like R-1 (cf. Fig. A.12) is characteristic for Al_2O_3 materials. Employing R-2 or R-3, which are more likely those to be observed for Si_3N_4 [21,30,31,55], it could still be calculated that their intersects (colour-coded dots) are beyond the threshold intersects for both of the Si_3N_4 materials (black dots). For comparison, the fitted R-curves of Si_3N_4-GP and Si_3N_4-PU were added in Fig. A.12 as dot-lines. Both are in good agreement with the theoretical curves R-2 and R-3.

The above considerations show that for materials with a steep or mild R-curve the critical load does not drop immediately after the crack initiation. Consequently, stable crack growth can be realised in theory, even when the experimental notch depth falls short of the theoretical threshold notch depth. That effectively allows for a wider absolute range of the stable crack extension, if desired.

Appendix B. Load drift correction

For the evaluation of either the R-curve or the subcritical crack growth (vK_I-relation), the machine raw data has to be refined and processed. The first step is related to the used testing equipment and may lapse/change for testing equipments other than the one used in the presented set up. This first step of data processing refers to the drift in the recorded load F_{exp}. The drift becomes visible by plotting F_{exp} vs. t, as done in Fig. B.14(a).

The graph can be understood as all individual load sequences stringed together. The long limbs of data points represent the complete unloading. In the presented experimental set up, complete unloading must always end at a minimum load of 2.9 N, which stems from the dead-weight F_d of the upper support, partially counteracted by the position encoders. However, that is not the case (visible from Fig. B.14(a)). For drift correction, the trace of the minimum points (black dots in Fig. B.14(a)) can be fitted by a polynomial function according to Eq. (B.1), typically using a fourth degree polynomial ($k = 4$).

$$F_{min}(t) = \sum_{j=0}^{k} p_j t^j \tag{B.1}$$

The coefficient of determination R^2 was acceptably high within the time range of an experiment and usually exceeded a level of 0.99. An extrapolation or generalisation of $F_{min}(t)$ is not possible, since the drift in the load varies from measurement to measurement. By restraining the degree of the fit polynomial, oscillation between the interpolation points can be avoided [14,18]. For the final drift correction, Eq. (B.2) was applied [14,18]. The entire load data F_{exp} was thus corrected for the two affecting contributions: the time-dependent drift of the load

$F_{min}(t)$ and the resulting dead weight F_d of 2.9 N.[5] It is now referred to as F. The effect of load drift correction is presented in Fig. B.14(b) and (c).

$$F = F_{exp} - (F_{min}(t) - F_d) \tag{B.2}$$

References

[1] R. Danzer, T. Lube, P. Supancic, R. Damani, Fracture of ceramics, Adv. Eng. Mater. 10 (4) (2008) 275–298.
[2] D. Munz, T. Fett, Ceramics mechanical properties, failure behaviour, materials selection, 1. Auflage, Springer Ser. Mater. Sci. 36 (2001) 25–26.
[3] D. Gross, T. Seelig, Bruchmechanik, Springer Berlin Heidelberg New York, 2006.
[4] R.W. Steinbrech, A. Reichl, W. Schaarwächter, R-curve behavior of long cracks in alumina, J. Am. Ceram. Soc. 73 (7) (1990) 2009–2015.
[5] M.E. Launey, R.O. Ritchie, On the fracture toughness of advanced materials, Adv. Mater. 21 (2009) 2103–2110.
[6] T. Fett, D. Munz, Subcritical crack growth of macrocracks in alumina with R-curve behavior, J. Am. Ceram. Soc. 75 (4) (1992) 958–963.
[7] C.J. Gilbert, R.N. Petrany, R.O. Ritchie, R.W. Steinbrech, Cyclic fatigue in monolithic alumina: mechanisms for crack advance promoted by frictional wear of grain bridges, J. Mater. Process. Technol. 30 (1995) 643–654.
[8] H. El Attaoui, M. Saadaoui, J. Chevalier, G. Fantozzi, Quantitative analysis of crack shielding degradation during cyclic fatigue of alumina, J. Am. Ceram. Soc. 178 (1) (2005) 172–178.
[9] E. Skiera, J. Malzbender, J. Mo, S. Dudczig, C.G. Aneziris, R.W. Steinbrech, Controlled crack propagation experiments with a novel alumina-based refractory, Adv. Eng. Mater. 14 (4) (2011) 248–254.
[10] T. Lube, R. Baierl, Sub-critical crack growth in alumina - a comparison of different measurement and evaluation methods, Berg- Und Hüttenmännische Monatshefte 156 (11) (2011) 450–456.
[11] R. Gutkin, M. Laffan, S. Pinho, P. Robinson, P. Curtis, Modelling the R-curve effect and its specimen-dependence, Int. J. Solids Struct. 48 (11) (2011) 1767–1777.
[12] C. Brokmann, S. Kolling, J. Schneider, Subcritical crack growth parameters in glass as a function of environmental conditions, Glas. Struct. Eng. 6 (2021) 89–101.
[13] R Core Team, R: A Language and Environment for Statistical Computing, R Foundation for Statistical Computing, Vienna, Austria, 2024.
[14] M. Lugovy, N. Orlovskaya, M. Neumann, C.G. Aneziris, H. Jelitto, G.A. Schneider, J. Kuebler, Room temperature R-curve and stable crack growth behaviour of ZrB_2-SiC ceramic composites, Adv. Appl. Ceram. 118 (4) (2019) 169–182.
[15] M. Neumann, J. Hubálková, F. Kerber, P. Gehre, H. Jelitto, C. Aneziris, Impact of thermal shock on the R-curve and subcritical damage behaviour of flame-sprayed alumina compounds, J. Eur. Ceram. Soc. 44 (2024) 3418–3428.
[16] H. Jelitto, F. Hackbarth, H. Özcoban, G.A. Schneider, Automated control of stable crack growth for R-curve measurements in brittle materials, Exp. Mech. 53 (2) (2013) 163–170.
[17] T. Fett, E. Diegele, Indirect measurements of compliance in four-point-bending tests, J. Test. Eval. 16 (1988) 487–488.
[18] M. Neumann, P. Gehre, J. Kuebler, N. Dadivanyan, H. Jelitto, G.A. Schneider, C.G. Aneziris, Stable crack propagation in free standing thermal sprayed al_2o_3 and Al_2O_3-ZrO_2-TiO_2 coatings, Ceram. Int. 45 (7) (2019) 8761–8766.
[19] H. Özcoban, V. Salikov, H. Jelitto, G.A. Schneider, Experimental crack front investigation of unpoled soft lead zirconate titanate (PZT) using the single edge V-Notched beam (SEVNB) method, Exp. Mech. 52 (9) (2012) 1565–1568.
[20] H. Jelitto, F. Felten, M.V. Swain, H. Balke, G.A. Schneider, Measurement of the total energy release rate for cracks in PZT under combined mechanical and electrical loading, J. Appl. Mech. 74 (6) (2007) 1197–1211.
[21] S. Fünfschilling, T. Fett, M. Hoffmann, R. Oberacker, T. Schwind, J. Wippler, T. Böhlke, H. Özcoban, G. Scheider, P. Becher, J. Kruzic, Mechanisms of toughening in silicon nitrides: The roles of crack bridging and microstructure, Acta Mater. 59 (2011) 3978–3989.
[22] H. Hübner, W. Jillek, Sub-critical crack extension and crack resistance in polycrystalline alumina, J. Mater. Sci. 12 (1) (1977) 117–125.
[23] T. Fett, D. Munz, G. Thun, Evaluation of bridging parameters in aluminas from R-curves by use of the fracture mechanical weight function, J. Am. Ceram. Soc. 78 (4) (1995) 949–951.
[24] H.E. Lutz, M.V. Swain, Interrelation between flaw resistance, R-curve behavior, and thermal shock strength degradation in ceramics, J. Eur. Ceram. Soc. 74 (11) (1991) 2859–2868.
[25] G. Vekinis, M.J. Ashby, P.W.R. Beaumont, R-curve behaviour of Al_2O_3 ceramics, Acta Met. et Mater. 38 (6) (1990) 1151–1162.
[26] N. Ramachandran, D. Shetty, Rising crack-growth-resistance (R-curve) behavior of toughened alumina and silicon nitride, J. Am. Ceram. Soc. 74 (10) (1991) 2634–2641.
[27] C. Li, D. Lee, S. Lui, R-curve behavior and strength for in-situ reinforced silicon nitrides with different microstructures, J. Am. Ceram. Soc. 75 (7) (1992) 1777–1785.
[28] Y. Kim, M. Mitomo, N. Hirosaki, R-curve behaviour of sintered silicon nitride, J. Mater. Sci. 30 (1995) 4043–4048.
[29] T. Fett, S. Fünschilling, M. Hoffmann, R. Oberacker, H. Jelitto, G. Schneider, R-curve determination for the initial stage of crack extension in Si_3N_4, J. Am. Ceram. Soc. 91 (11) (2008) 3638–3642.
[30] S. Fünfschilling, T. Fett, M.J. Hoffmann, R. Oberacker, H. Jelitto, G.A. Schneider, M. Härtelt, H. Riesch-Oppermann, Bridging stresses from R-curves of silicon nitrides, J. Mater. Sci. 44 (2009) 3900–3904.
[31] S. Fünfschilling, T. Fett, M.J. Hoffmann, R. Oberacker, H. Jelitto, G.A. Schneider, Determination of the crack-tip toughness in silicon nitride ceramics, J. Mater. Sci. 44 (2009) 335–338.
[32] M. Härtelt, S. Fünfschilling, T. Schwind, H. Riesch-Oppermann, T. Fett, J. Kruzic, Deducing the fatigue crack growth rates of natural flaws in silicon nitride ceramics: Role of R-curves, J. Am. Ceram. Soc. 96 (8) (2013) 2593–2597.
[33] H. Özcoban, H. Jelitto, G.A. Schneider, Influence of finite notch root radius and optically determined crack length on the measured fracture toughness of brittle materials, J. Eur. Ceram. Soc. 30 (2010) 1579–1583.
[34] R. Damani, R. Gstrein, R. Danzer, Critical notch-root radius effect in SENB-s fracture toughness testing, J. Eur. Ceram. Soc. 16 (1996) 695–702.
[35] T. Fett, Influence of a finite notch root radius on fracture toughness, J. Eur. Ceram. Soc. 25 (2005) 543–547.
[36] M. Inagaki, K. Urashima, s. Toyomasu, Y. Goto, M. Sakai, Work of fracture and crack healing in glass, J. Am. Ceram. Soc. 68 (12) (1985) 704–706.
[37] M. Soga, Elastic moduli and fracture toughness of glass, J. Non-Cryst. Solids 73 (1985) 305–313.
[38] G. Quinn, J. Swab, Fracture toughness of glasses as measured by the SCF and SEPB methods, J. Eur. Ceram. Soc. 37 (2017) 4243–4257.
[39] T. To, L. Jensen, M. Smedskjaer, On the relation between fracture toughness and crack resistance in oxide glasses, J. Non-Cryst. Solids 534 (2020) 119946.
[40] A. Evans, A method for evaluating the time-dependent failure characteristics of brittle materials - and its application to polycrystalline alumina, J. Mater. Sci. 7 (1972) 1137–1146.
[41] K.E. Aeberli, R.D. Rawlings, Effect of simulated body environments on crack propagation in alumina, J. Mater. Sci. Lett. 2 (5) (1983) 215–220.
[42] M.J. Reece, F. Guiu, M.F.R. Sammur, Cyclic fatigue crack propagation in alumina under direct tension - compression loading, J. Am. Ceram. Soc. 72 (2) (1989) 348–352.
[43] T. Fett, G. Martin, D. Munz, G. Thun, Determination of da/dN-ΔK1 curves for small cracks in alumina in alternating bending tests, J. Mater. Sci. 26 (12) (1991) 3320–3328.
[44] T. Fett, W. Hartlieb, K. Keller, B. Knecht, D. Munz, W. Rieger, Subcritical crack growth in high-grade alumina, J. Nucl. Mater. 184 (1991) 39–46.
[45] R. Ritchie, R. Dauskardt, Cyclic fatigue of ceramics a fracture mechanics approach to subcritical crack growth and life prediction, J. Ceram. Soc. Japan 99 (10) (1991) 1047–1062.
[46] G. Choi, Cyclic fatigue crack growth in silicon nitride: Influences of stress ratio and crack closure, Acta Met. et Mater. 43 (4) (1995) 1489–1494.
[47] C. Gilbert, R. Dauskardt, R. Ritchie, Microstructural mechanisms of cyclic fatigue-crack propagation in grain-bridging ceramics, Ceram. Int. 23 (1997) 413–418.
[48] M. Lengauer, R. Danzer, Silicon nitride tools for the hot rolling of high-alloyed steel and superalloy wires - crack growth and lifetime prediction, J. Eur. Ceram. Soc. 28 (2008) 2289–2298.
[49] R. Greene, S. Fünfschilling, T. Fett, M. Hoffmann, J. Kruzic, Fatigue crack growth behavior of silicon nitride: Roles of grain aspect ratio and intergranular film composition, J. Am. Ceram. Soc. 96 (1) (2013) 259–265.
[50] T. Fett, D. Munz, K. Keller, Determination of subcritical crack growth on glass in water from lifetime measurements on knoop-cracked specimens, J. Mater. Sci. Lett. 23 (1988) 798–803.
[51] T. Fett, G. Martin, D. Munz, v-K curves for borosilicate glass obtained from static bending tests with cracks introduced by the bridge method, J. Mater. Sci. Lett. 10 (1991) 220–222.
[52] T. Fett, K. Germerdonk, A. Grossmüller, K. Keller, D. Munz, Subcritical crack growth and threshold in borosilicate glass, J. Mater. Sci. Lett. 26 (1991) 253–257.
[53] S. Weiderhorn, H. Johnson, A. Diness, A. Heuer, Fracture of glass in vacuum, J. Am. Ceram. Soc. 57 (8) (1974) 336–341.
[54] T. Suratwala, R. Steele, Anomalous temperature dependence of sub-critical crack growth in silica glass, J. Non-Cryst. Solids 316 (2003) 174–182.
[55] S. Fünfschilling, T. Fett, R. Oberacker, M. Hoffmann, H. Özcoban, H. Jelitto, G. Schneider, J. Kruzic, R curves from compliance and optical crack-length measurements, J. Am. Ceram. Soc. 93 (9) (2010) 2814–2821.
[56] J. Nakayama, H. Abe, R. Bradt, Crack stability in the work-of-fracture test refractory applications, J. Am. Ceram. Soc. 64 (11) (1981) 671–675.
[57] H. Özcoban, Hochpräzise R-Kurven- und schnelle v-K_I-Kurven-Messung an Keramiken mittels einer steifen, computergeregelten Biegeapparatur (Ph.D. thesis), Hamburg University of Technology, 2012.

[5] In case of the glass sample, a lighter upper support was used, resulting in a dead weight of $F_d = 1.1$ N